## nature water

**Article** 

https://doi.org/10.1038/s44221-022-00003-2

# Nanosecond bacteria inactivation realized by locally enhanced electric field treatment

Received: 29 March 2022

Accepted: 31 October 2022

Published online: 12 January 2023

Check for updates

Ting Wang<sup>1</sup> & Xing Xie **©** <sup>1,2</sup> ⊠

Bacterial contamination in water is still a critical threat to public health; seeking efficient water disinfection approaches is of great significance. Here we show that locally enhanced electric field treatment (LEEFT) by electrodes modified with nanoscale tip structures can induce ultrafast bacteria inactivation with nanosecond electrical pulses. A lab-on-a-chip device with gold nanowedges on the electrodes is developed for an operando investigation. Attributed to the lightning-rod effect, the bacteria at the nanowedge tips are inactivated by electroporation. A single 20 ns pulse at 55 kV cm<sup>-1</sup> has achieved 26.6% bacteria inactivation, with ten pulses at 40 kV cm<sup>-1</sup> resulting in 95.1% inactivation. LEEFT lowers the applied electric field by about 8 fold or shortens the treatment time by at least 10<sup>6</sup> fold, compared with the system without nanowedges. Both Gram-positive and Gram-negative bacteria, including antibiotic-resistant bacteria, are inactivated with nanosecond pulses by LEEFT. According to simulation, when the membrane of the cell located at the nanowedge tip is directly charged by the concentrated charges at the tip, it is charged much faster and to a much higher level, leading to instant electroporation and cell inactivation.

Public health is threatened by a wide variety of pathogenic water contamination. More than 650 million people around the world still lack access to clean water<sup>1</sup>. The importance of finding effective water disinfection methods cannot be overstated. The action speed is a major parameter indicating the efficacy of a water disinfection method, since higher speeds allow higher flow rates and lower hydraulic retention times. Antibacterial agents, such as metal ions and compounds, are intensively studied for their antimicrobial applications in water<sup>2,3</sup>. They act by interrupting cell functionalities, such as causing protein dysfunction, oxidative stress and genotoxicity, which takes place at a timescale of minutes to hours<sup>4,5</sup>. A silver nanocluster packed with daptomycin was reported to cause 84% Staphylococcus aureus cell damage after 2 h of incubation at the concentration equivalent to 10 µM daptomycin and 200 µM Ag (ref. 6).

The stronger oxidants used in water disinfection, such as free chlorine and ozone, have faster antimicrobial effects on microbes. They damage the cell structure via direct oxidation or generation of reactive oxygen species (ROS)7. The CT values (that is, the product of concentration and hydraulic retention time) of these disinfection methods indicate a trade-off between the treatment time and disinfectant dose: to shorten the treatment time, a higher dosage is necessary. The treatment time to achieve 99% inactivation of Escherichia coli is 10 s and 0.1 s using 6 mg l<sup>-1</sup> free chlorine and 5 mg l<sup>-1</sup> ozone (the highest typical doses), respectively. Most other pathogenic bacteria and protozoa are more resistant than E. coli<sup>7</sup>.

Although chemical-based approaches are widely used in water disinfection, they cause problems such as generating carcinogenic disinfection by-products and inducing antimicrobial resistance<sup>8–10</sup>. Therefore, alternative physical methods are also investigated, such as using ultraviolet (UV), thermal treatment and electric field treatment. UV at around 260 nm can damage bacteria DNA by dimerizing thymine molecules, inhibiting transcription of genetic code and preventing its reproduction. The dosage for 99% inactivation of bacteria and viruses ranges from 5 mW  $s^{\text{--}1}\,\text{cm}^2$  to 25 mW  $s^{\text{--}1}\,\text{cm}^2$  , meaning that with a typical UV intensity of 5 mW cm<sup>-2</sup>, the required exposure time is at least 1 s (refs. 7,11). Another light-related method, photocatalysis, inactivates waterborne microbes through a photocatalytic redox mechanism relying on photocatalytic materials, such as TiO<sub>2</sub>. At least

School of Civil and Environmental Engineering, Georgia Institute of Technology, Atlanta, GA, USA. Institute for Electronics and Nanotechnology, Georgia Institute of Technology, Atlanta, GA, USA. e-mail: xing.xie@ce.gatech.edu

tens of minutes are used to achieve 99% disinfection<sup>12</sup>. Heat acts to kill bacteria by denaturation of proteins and nucleic acids. For thermal processing, 1 min at 65 °C is necessary to inactive 90% of most waterand food-borne pathogens<sup>13</sup>. In conventional electric field treatment (CEFT) processes, high-voltage electrical pulses are applied between two parallel plate electrodes to generate a strong electric field, which induces irreversible electroporation that damages the cell membrane and thus cell inactivation<sup>14</sup>. Pulses with micro- to millisecond durations are already capable of inducing cell inactivation, which has pushed the action speed to the subsecond region<sup>14</sup>.

As the action speed is critical to the disinfection method, it is intriguing to know what the minimum time is needed to inactivate bacteria and by which method. Antimicrobial agents usually need a relatively long time since they inhibit bacteria by disturbing their microbiology processes. The action speed of oxidants is limited by the mass transfer and kinetics of the redox reactions. The physical methods can be faster, such as electroporation, where the pore formation on the membrane needs only a few nanoseconds after a sufficient transmembrane voltage (TMV) is built up 15,16. However, building up the TMV usually requires tens to hundreds of microseconds, which becomes the major speed limitation. That is why electrical pulses with microto millisecond pulse width are currently used in CEFT. Furthermore, an extremely high applied voltage (typically several tens of kilovolts) is required in CEFT, which leads to safety concerns and high energy consumption, thus largely hindering its wide application 14,17.

In this Article, we push the bacteria inactivation time to the nanosecond scale using locally enhanced electric field treatment (LEEFT). LEEFT is improved from CEFT by decorating the electrodes with nanoscale tip structures, which can locally enhance the electric field by lightning-rod effect and reduce the applied voltages<sup>18</sup>. As charges are concentrated at the nanoscale tips, we hypothesize that LEEFT can charge the cell membrane much faster than CEFT and break the charging time limit, thus inducing ultrafast electroporation. LEEFT with low-voltage direct current and alternating current has demonstrated superior performance for water and aerosol disinfection 19-28. Recently, an operando investigation of LEEFT with microsecond pulses illustrated that electroporation is the predominant mechanism<sup>18</sup>. Nevertheless, the antimicrobial effect of LEEFT with nanosecond pulses has not been discovered before. Here we achieve ultrafast nanosecond bacteria inactivation using LEEFT. We have developed a LEEFT platform with lab-on-a-chip devices to conduct operando investigations, demonstrated the ultrafast nanosecond antimicrobial effect at the single-cell level and illustrated its mechanisms. The results show that nanosecond LEEFT has significant advantages over CEFT by both shortening the treatment time and lowering the applied electric field. The cell located at the nanoscale tip is charged instantly by the charges concentrated at the tip, which induces rapid electroporation and bacteria inactivation. Thus, using LEEFT, we demonstrate and characterize nanosecond bacteria inactivation.

## Bacteria inactivation achieved by nanosecond pulses

A lab-on-a-chip is developed for the operando investigation. Two gold electrodes with gold nanowedges are deposited on the chip surface. The model bacteria *Staphylococcus epidermidis* are uniformly immobilized on the chip and immersed in de-ionized (DI) water (Fig. 1a and Supplementary Fig. 1). When a voltage is applied, the electric field near the nanowedge tips is greatly enhanced due to the lightning-rod effect. The applied electric field is 55 kV cm<sup>-1</sup> when 138 V is applied across a 25 µm electrode gap, and simulation shows that the nano-enhanced electric field achieved at the nanowedge tips can be ~400 kV cm<sup>-1</sup> (Fig. 1b). A live/dead cell viability stain propidium iodide (PI) is added to the water before treatment. When pores form on the cell membrane, the cell is stained with PI and shows red fluorescence. The fluorescence changing of individual cells after a single 20 ns pulse at 55 kV cm<sup>-1</sup> applied electric field is shown in Fig. 1c. All cells have a dye inflow (fluorescence

increase) to some extent right after the pulse, but some cells maintain a low intensity for up to 10 s until the fluorescence finally spikes. Although pores are induced on the membrane by the single pulse, some pores may close quickly within milliseconds after the pulse, thus limiting further dye diffusion into the cell and delaying the fluorescence spike<sup>15</sup>. No significant difference is found between the cells located at the positive and negative electrodes. The microscopy images at different timepoints show that the dye diffuses into the cell from the nanowedge tip, indicating that the cell damage is directly induced by the nanowedge (Fig. 1c).

To distinguish reversible cell damage and cell inactivation, a double staining method is used. Another live/dead cell viability stain, SYTOX Green, is first added to the medium before treatment to determine total cell damage (green fluorescence). Twenty minutes after the treatment, PI is then added to stain the inactivated cells (Supplementary Fig. 2). Reversible pores should already close within the 20 min window, so the cells also stained with PI (show orange or red colour) are considered to have permanent cell damage and be inactivated  $^{15,29}$ . After a single 20 ns pulse at 55 kV cm $^{-1}$ , 59.7% and 26.6% nanowedges at the positive electrodes achieved bacteria damage and inactivation, respectively. After ten pulses are applied at 40 kV cm $^{-1}$ , the percentages increase to 98.8% and 95.1%. The nanowedges at the negative electrodes show similar performance (Fig. 1d).

The side-by-side comparison of the optical microscopy and scanning electron microscopy (SEM) image (Fig. 1e and Supplementary Fig. 3) shows that some inactivated cells are flattened and have cytoplasm release (red arrows), while some other inactivated cells still maintain their original structure (white arrows). The flattened cells show intracellular compound release but not severe cell membrane damage, indicating the cell inactivation is due to membrane permeability increase at one point but not whole-cell oxidation or degradation of the cells being inactivated but still maintaining a good structure, no pores are observed. The electroporation pores have sizes at nanometre scale and are at most metastable, and are thus too fragile to withstand the sample preparation required for SEM imaging 15.

The non-connected nanowedges could also induce ultrafast bacteria inactivation with nanosecond pulses. Three rows of nanowedges (8  $\mu m$  length, 200 nm tip width and 1  $\mu m$  middle width) have been fabricated between the positive and negative electrodes (Fig. 1f). The simulation shows that the electric field could be enhanced at both tips. After  $10^6$  pulses (20 ns pulse width at 14 kV cm $^{-1}$ ) are applied, 70.1% and 52.7% nanowedges achieve bacteria damage and inactivation, respectively, at the positive side tips (pointing up), and 72.4% and 47.7% at the negative side tips (Fig. 1f,g). When smaller tip structures (4  $\mu m$  long and 200 nm wide) are densely arranged, a larger number of bacteria could be inactivated (Fig. 1h), suggesting that an antimicrobial and biofilm inhibition surface could be developed. Nevertheless, there is a trade-off between the nanotip arranging density and electric field enhancement, where the nano-enhanced electric field will decrease when the horizontal interval between the nanotips is smaller (Supplementary Fig. 4).

#### **LEEFT enables ultrafast bacteria inactivation**

The antimicrobial performance of LEEFT is compared with that of CEFT (without nanowedges) at three different pulse widths (20, 200 and 2,000 ns) (Fig. 2a,b). The antimicrobial efficiency of LEEFT is represented by the percentage of nanowedges that achieve bacteria damage/inactivation. The antimicrobial efficiency of CEFT is the percentage of cells damaged/inactivated between the two electrodes (Supplementary Fig. 5). The duty cycle is 0.1% (pulse width/period = 0.1%), and the effective treatment time (that is, the product of pulse width and pulse number) is 20 ms for all three pulse widths. With 2,000 ns pulses, >95% bacteria inactivation is achieved at 40 kV cm $^{-1}$  applied electric field in CEFT (Fig. 2a). In LEEFT, similar inactivation efficiency is achieved at 12 kV cm $^{-1}$ , demonstrating over three-fold reduction in the applied electric field, which is attributed to the electric field enhancement at

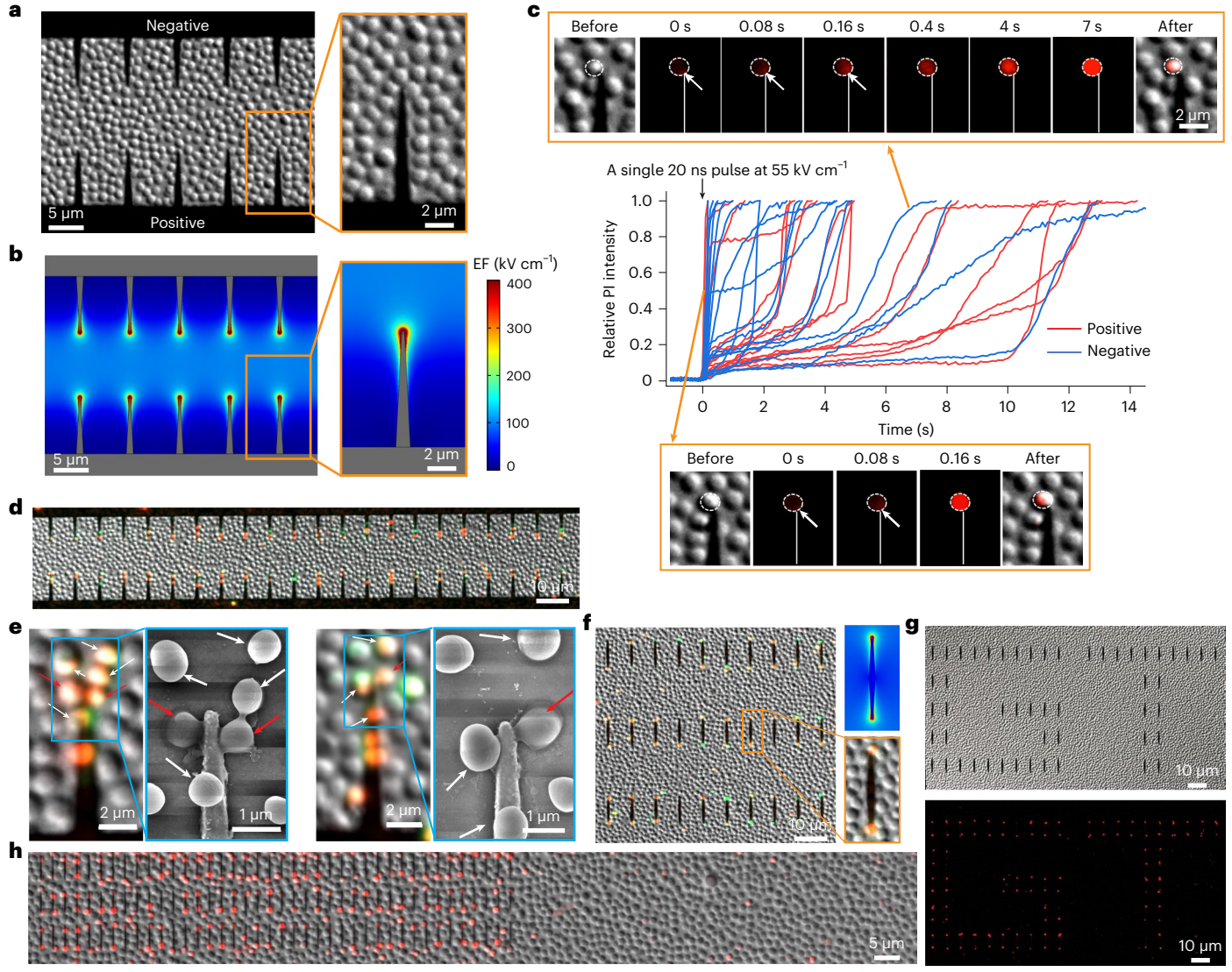


**Fig. 1**| **Bacteria inactivation by nanosecond pulses at the nanowedge tips. a**, The model bacteria *S. epidermidis* are immobilized on the chip. **b**, The simulated nano-enhanced electric field under 55 kV cm<sup>-1</sup> applied electric field. **c**, The relative PI intensity of individual cells after a single pulse is applied. Each line represents a single cell located at the nanowedge tip on either the positive or the negative electrode. The microscopy images show the PI dye diffusion pattern. **d**, Bacteria inactivation after LEEFT (20 ns pulse, 40 kV cm<sup>-1</sup>, ten pulses). The red and orange cells are inactivated cells stained with PI. **e**, Side-by-side comparison of optical microscopy and SEM images after LEEFT (20 ns pulse,

55 kV cm<sup>-1</sup>, ten pulses). The red arrows indicate the flattened cells, while the white arrows indicate the inactivated cells that still maintain a good shape. **f**, Bacteria inactivation achieved by non-connected nanowedges, and the simulation of the nano-enhanced electric field. **g**, Bacteria inactivation at the nanowedge tips that are arranged in a 'GT' pattern. Top: DIC channel microscopy image before LEEFT. Bottom: fluorescence channel microscopy image after LEEFT. **h**, Bacteria inactivation achieved by densely packed nanotips. The inactivated cells in **g** and **h** are only indicated by PI stain and show red fluorescence.

the nanowedge tips (Fig. 2b). For shorter pulses, the advantage of LEEFT is further revealed. The antimicrobial efficiency drops dramatically in CEFT as the pulses are shortened (Fig. 2a). Only 0.89% inactivation is found with 20 ns pulses at 40 kV cm<sup>-1</sup>. On the contrary, LEEFT shows only a slight decrease in antimicrobial efficiency when the pulses are shortened to 20 ns (Fig. 2b). This result indicates that 20 ns pulses are too short to charge the cells in the bulk space (in CEFT) but are almost long enough to induce electroporation on the cells located at the nanowedge tip (in LEEFT).

The bacteria inactivation by LEEFT and CEFT with 20 ns pulses at different effective treatment times (different pulse numbers) are shown in Fig. 2c,d. With 20 ms effective treatment, 37% nanowedges induce bacteria damage under 7 kV cm $^{-1}$  in LEEFT (Fig. 2c), which is higher than 19.4% in CEFT under 55 kV cm $^{-1}$  (Fig. 2d), indicating an eightfold decrease of the applied electric field in LEEFT. At 55 kV cm $^{-1}$ ,

CEFT achieved 10% bacteria inactivation after 200 ms effective treatment time, while LEEFT achieved 97.1% with 200 ns, which is 106 times shorter. This result shows the significant advantage of LEEFT in terms of shortening the treatment time and reducing the applied electric field. For nanosecond LEEFT, by slightly increasing the applied electric field, the effective treatment time can be shortened by several orders (Fig. 2d). Therefore, applying a stronger electric field can greatly reduce the overall energy consumption (Supplementary Fig. 6 and Supplementary Section 2.1).

For an antibiotic-resistant strain of *S. epidermidis*, LEEFT achieves similar bacteria inactivation performance as the regular strain (Fig. 2e,f). This could be explained by the mechanism of electroporation where the pores are induced on the lipid bilayer, and the two strains have the same basic structure of lipid bilayers. The inactivation efficiency of Gram-negative bacteria *E. coli* is lower than the Gram-positive

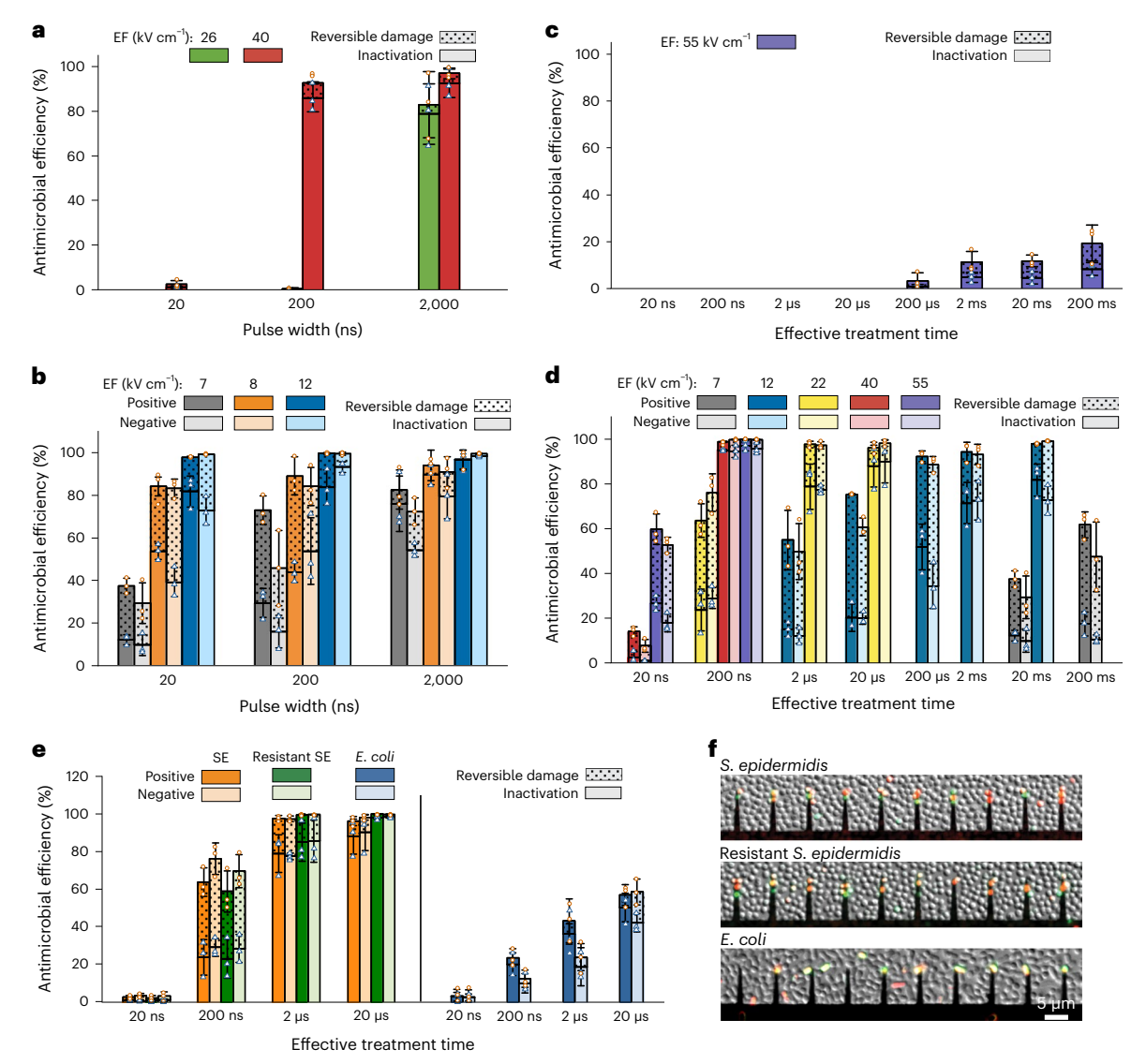


**Fig. 2** | **Antimicrobial performance of LEEFT. a,b**, Antimicrobial efficiency of CEFT (**a**) and LEEFT (**b**) under different pulse widths. EF (kV cm<sup>-1</sup>) represents the applied electric field (EF = applied voltage/distance separating the electrodes). The effective treatment time and duty cycle are fixed at 20 ms and 0.1%. **c,d**, Antimicrobial efficiency of CEFT (**c**) and LEEFT (**d**) subjected to 20 ns pulses at different effective treatment times. The duty cycle is 0.1% (20 μs period and 50 kHz). **e**, Antimicrobial efficiency of LEEFT on *S. epidermidis* (SE), antibiotic-

resistant *S. epidermidis* (resistant SE) and *E. coli* treated with 20 ns pulses at 22 kV cm<sup>-1</sup>. In **a–e**, data are presented as mean values. Error bars represent the s.d. from n=3 replicates. The dot plots represent raw data of total bacteria damage (red circles) and bacteria inactivation (blue triangles). **f**, Microscopy images of the bacteria after LEEFT with 20 ns pulses at 22 kV cm<sup>-1</sup> after 20  $\mu$ s effective treatment time.

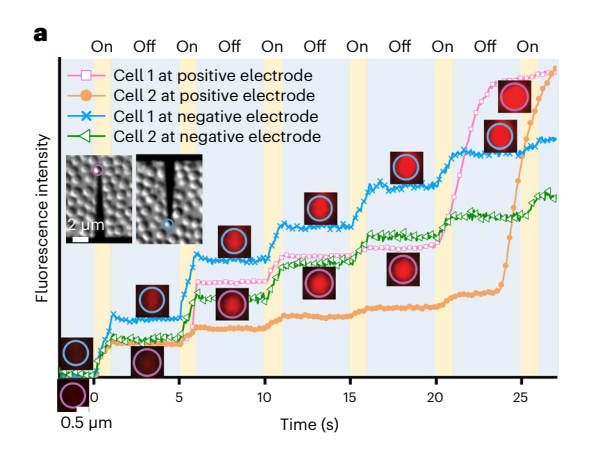
*S. epidermidis* (Fig. 2e,f). As they have different cell wall structures, the lethal electroporation threshold may be different <sup>31</sup>. Gram-positive bacteria have thicker cell walls because of a thick peptidoglycan layer outside the lipid bilayer membrane, which is usually used to explain their higher resistance to mechanical and oxidation disruption compared with Gram-negative bacteria <sup>32–36</sup>. Although Gram-negative bacteria have thinner cell walls, they have two sets of lipid bilayers. As LEEFT kills bacteria via causing electroporation on the lipid bilayer, the additional set of lipid bilayers may explain the higher resistance of *E. coli* to LEEFT over *S. epidermidis*.

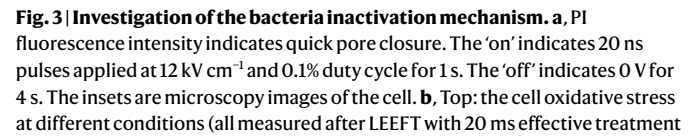
## The bacteria inactivation is induced by electroporation

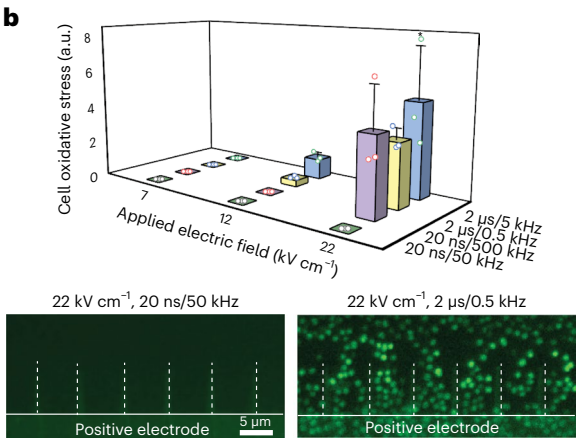
Our previous work demonstrated that electroporation is the predominant mechanism for bacteria inactivation in LEEFT<sup>18</sup>. Here we find reversible electroporation under nanosecond pulses, confirming that the bacteria inactivation by nanosecond pulses is also caused

by electroporation. Each line in Fig. 3a represents the PI uptake of an individual cell at the nanowedge tip. The cells are subjected to intermittent treatment, where 20 ns pulses are applied at 12 kV cm<sup>-1</sup> and 0.1% duty cycle for 1 s (the yellow area), and then turned off for 4 s (the blue area). The fluorescence increases when the pulses are applied, suggesting pore formation and dye inflow. When the pulses are removed, the fluorescence stops increasing immediately, indicating quick pore closure and membrane recovery. This process can be repeated several times unit the cell is eventually inactivated. This phenomenon is also found in cells located at the tips of non-connected nanowedges (Supplementary Fig. 7). The rapid membrane recovery is common in electroporation but not in other kinds of cell damage, such as thermal treatment or oxidation, indicating that electroporation is induced in LEEFT and can cause bacteria inactivation.

To investigate whether there is ROS or oxidation damage induced by the electrical pulses, the cell oxidative stress is detected using a fluorescence probe DCFH-DA. The dye is widely used to detect cellular







time). The asterisk denotes bubble formation. Data are presented as mean values. Error bars represent the s.d. from n=3 replicates. The dot plots represent the corresponding raw data. Bottom: the green fluorescence of DCFH-DA showing the oxidative stress in cells near the positive electrode.

ROS levels<sup>37,38</sup>. No oxidative stress is detected under 20 ns pulses at 22 kV cm<sup>-1</sup> and 50 kHz (0.1% duty cycle) even after 20 ms effective treatment time (Fig. 3b), but >80% bacteria inactivation has already been achieved at 22 kV cm<sup>-1</sup> with 20 µs effective treatment time (as shown in Fig. 2d), suggesting that the bacteria inactivation is not due to oxidation. Additionally, even when notable oxidative stress is detected by DCFH-DA in some cells (for example, 20 ns/500 kHz at 22 kV cm<sup>-1</sup>), it does not necessarily cause bacteria inactivation (Supplementary Fig. 8). This further supports that the bacteria inactivation achieved without detected oxidative stress should be solely due to electroporation. Furthermore, the cell membrane peroxidation is measured using BODIPY 581/591 C11 reagent, and no membrane peroxidation is detected under 20 ns pulses when ~90% bacteria inactivation has been achieved (Supplementary Fig. 9)<sup>39</sup>. Cell damage due to water ionization and bubble formation is also ruled out (Supplementary Section 2.2). Compared with 2 µs pulses, 20 ns pulses induce less oxidative stress under the same applied electric field and higher frequencies, indicating that applying nanosecond pulses is more pristing than using long pulses, therefore inducing less side reaction and generating fewer disinfection by-products (Supplementary Section 2.3).

## Proposed mechanism of the ultrafast electroporation

According to the mechanism of electroporation, charged ions in the extracellular medium and cytoplasm will migrate under the external electric field, accumulate at the two sides of the cell membrane and build up the TMV, thus inducing electroporation (Supplementary Fig. 10a). Charging the cell membrane is like charging a capacitor in a circuit. In a medium with a relatively low conductivity, the charged ions travel slower in the medium, so a longer time is needed to fully charge the membrane (corresponding to longer capacitor charging time with higher circuit resistance) (Supplementary Fig. 10b)<sup>40</sup>. Therefore, nanosecond pulses are usually considered impossible to induce electroporation in CEFT (Supplementary Section 2.4 and Fig. 10c,d).

Here we propose another membrane charging mechanism for cells at the nanowedge tip: instead of being charged by ions in water, the cell membrane is directly charged by the charges concentrated at the nanowedge tip (Fig. 4a). As the charges in the gold nanowedges travel much faster than the charged ions in the medium, the membrane could be fully charged almost instantly, thus inducing electroporation. The non-connected nanowedge could also be polarized by the external electric field, which causes quick cell electroporation at the tip.

To verify the proposed mechanism, the membrane charging process is simulated using a finite element method. The 3D models are built for cells 1, 2 and 3, which are between the two electrodes, on the surface of a flat electrode and at the nanowedge tip, respectively (Fig. 4b). The applied voltage reaches 60 V at 10 ns (12 kV cm<sup>-1</sup>). The TMV versus time shows that the cell at the nanowedge tip (cell 3) is charged much faster and to a much higher level than the cell in bulk (cell 1) (Fig. 4c). Cell 3 is charged to 87% at 100 ns, while only 23% is achieved for cell 1 (Supplementary Fig. 11). Cell 3 achieves up to 30 times higher TMV than cell 1 before 100 ns. After 10<sup>4</sup> ns, the ratio stabilizes at 7.5 (Fig. 4d). This demonstrates two types of enhancement that LEEFT achieves: increasing the charging speed and elevating the charging amplitude.

Cell 2 on the surface of a flat electrode is also charged fast (to 68% at 100 ns), but the final charging amplitude is similar to that of cell 1 (Fig. 4c and Supplementary Fig. 11). We use the TMV ratio of cell 2 to cell 1 to represent the role of direct cell–electrode contact, and the ratio of cell 3 to cell 2 to represent the role of nanowedges (Fig. 4d). The ratio of cell 2 to cell 1 falls to 1 after  $10^4$  ns, indicating that the direct cell–electrode contact contributes only to the higher charging speed but not the final charging amplitude. The ratio of cell 3 to cell 2 is higher than 10 before 100 ns and stays at 7 after  $10^4$  ns, suggesting that the nanowedges contribute to both higher terminal charging amplitude and higher charging speed.

We then evaluate the inner and outer cell membrane potential to further investigate the cell charging process. Compared with cell 2, the slow membrane charging of cell 1 is mainly due to the slow potential build-up of the outer membrane, which is due to the slow ion transportation in the extracellular medium (Fig. 4e). As cell 2 and cell 3 directly contact with the electrode, they have equal outer membrane potential with the electrode, which reaches 60 V at 10 ns. It is worth noting that the inner membrane potential of cell 3 is much lower than that of cell 2 (Fig. 4e). For the flat electrodes without nanowedges, the potential gradient between the positive and ground electrode should be uniform. As cell 2 contacts with the bulk electrode and the inner membrane is very close to the electrode (the membrane thickness is 50 nm), the inner potential is just slightly lower than 60 V, which is about 59.9 V. For cell 3, the long and thin nanowedge creates a highly non-uniform potential gradient near the tip, as shown by the potential contour in Fig. 4f. Therefore, at only 50 nm (membrane thickness) from the tip, the potential already drops to around 56 V, which becomes the initial inner potential of cell 3. From 10 ns to 100 ns, the inner potential further drops quickly, which could be explained

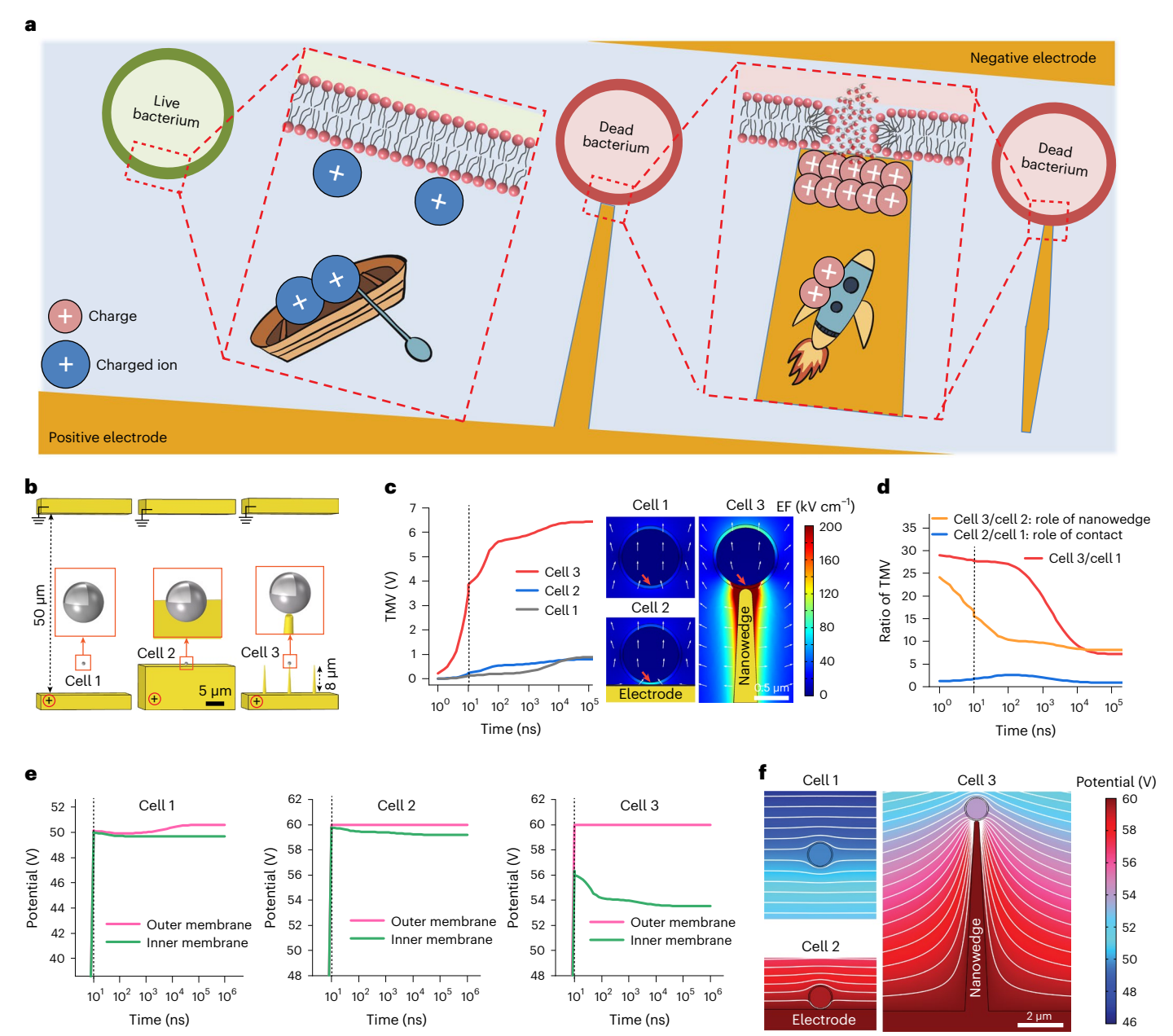


**Fig. 4** | **Theoretical analysis of the ultrafast cell electroporation in LEEFT. a**, Schematic of the membrane charging and electroporation. **b**, The 3D models of the simulation. Two concentric spheres of 1  $\mu$ m and 0.9  $\mu$ m in diameter are built to represent the outer and inner membrane of the cell. A part of the outer membrane is hidden in the enlarged image to show the two membranes. **c**, Left: TMV build-up with time. The dashed line indicates that the applied voltage reaches 60 V at 10 ns. Right: the simulation figures showing the membrane

charging amplitude (represented as the electric field strength) at 100 ns. The white arrows indicate the electric field direction. The red arrows indicate the position analysed in the left figure. **d**, The TMV ratio between cells 1, 2 and 3. **e**, Change of the inner and outer membrane potential with time. **f**, Potential distribution and the potential contour (white lines) plotted at an interval of 0.5 V at 100 ns.

by the quicker migration and accumulation of negative ions inside the cytoplasm due to the larger driving force from the larger initial TMV (Fig. 4e). In summary, the quick and high-amplitude membrane charging at the nanowedge tip occurs because the cell membrane is directly charged by the concentrated charges at the nanowedge tip. This matches our proposed membrane charging mechanism. Cells not directly contacting the nanowedge tip still need to be charged by the ions in the medium between the cell and the tip (Supplementary Section 2.5). Therefore, the direct cell–nanowedge contact guarantees the fastest membrane charging, which is critical for the nanosecond cell electroporation and inactivation in LEEFT.

## Discussion on strategies to improve LEEFT performance

As the effective zone of LEEFT (where the electric field is enhanced) is limited to about 2 µm from the nanowedge tips (Fig. 1b), LEEFT can be considered as a heterogeneous disinfection process. Similar to other heterogeneous processes, there are several ways to improve antimicrobial efficiency. Firstly, the electrodes can be covered with nanoscale tips with a relatively high density to increase the effective area. In our previous studies, we grew dense CuO or Cu<sub>3</sub>P nanowires on copper mesh electrodes for LEEFT water disinfection<sup>20–22,24,41</sup>. In addition, it is demonstrated that, under neutral pH, bacteria could be transported to the

nanoscale tips on both positive and negative electrodes<sup>18</sup>, probably due to the combination of electrophoretic and dielectrophoretic forces. The parameters of electrical pulses, such as pulse width, direction and voltage, could be altered to effectively manipulate cells in the flow and to drive bacteria cells towards the tips. Furthermore, mixing could be introduced to increase the possibility of bacteria touching the tips. Due to the ultrafast nanosecond bacteria inactivation in LEEFT, very quick contacts between the cells and the tips are sufficient to achieve effective bacteria inactivation, thus potentially leading to high water throughput and disinfection efficiency.

#### Conclusion

This work demonstrates ultrafast bacteria inactivation using nano-second electrical pulses in LEEFT. A single 20 ns pulse at 55 kV cm<sup>-1</sup> has achieved 26.6% bacteria inactivation, while ten pulses (total 200 ns) at 40 kV cm<sup>-1</sup> results in 95.1% inactivation. Compared with the system without nanowedges, the treatment time is shortened by at least 10<sup>6</sup> fold, or the applied electric field is lowered by about 8 fold to achieve similar bacteria inactivation in LEEFT. Because at the nanowedge tips the cell membrane can be directly charged by the concentrated charges, the TMV can reach 30-fold higher values than that of a cell in the bulk space within 100 ns. Such instant membrane charging induces rapid electroporation and, thus, bacteria inactivation.

#### **Methods**

#### Lab-on-a-chip fabrication and pre-treatment

A lab-on-chip is developed to visualize and characterize the bacteria inactivation of LEEFT. The chips were fabricated by depositing gold nanowedges and electrodes on a glass wafer substrate (Supplementary Fig. 1). Gold is both mechanically and electrochemically stable and has little antimicrobial effect. It is also widely used as electrodes or contact pads in microchips. The gold nanowedges have a width of 200 nm at the tip, which gradually increases to 1 µm at the base to allow a steadier connection to the bulk electrode. The thickness, length and interval of the nanowedges is 200 nm, 8 μm and 7 μm, respectively. The nanowedges were first defined using electron beam lithography and deposited by a lift-off method. Then, the 300-nm-thick bulk gold electrodes with 25 or 50 µm electrode separation gap were fabricated using the photo lithography and lift-off method. The fabricated chips were coated with poly-L-lysine for bacteria immobilization<sup>18</sup>. To reuse the chips, the used chips were washed with 5% bleach, 30% H<sub>2</sub>O<sub>2</sub> and DI water to remove the attached bacteria and the old poly-L-lysine, and recoated with poly-L-lysine. The detailed chip fabrication and pre-treatment methods are outlined in Supplementary Section 1.1.

#### Bacteria culture, collection and immobilization on the chip

The model bacteria *S. epidermidis* (ATCC 12228), the antibiotic resistant *S. epidermidis* (ATCC 700576) and *E. coli* (ATCC 10798) were cultured for 15 h in nutrient broth and LB broth, respectively. Four millilitres of the bacteria solution were washed three times with 10 mM phosphate buffer by centrifuging at 1,000 *g* for 5 min, and finally concentrated to 0.5 ml. A drop of the prepared bacteria suspension was added onto a poly-L-lysine coated chip to cover the gap between the two electrodes. After 50 min for the cells to settle down, a layer of bacterial cells were immobilized on the chip surface. The unattached cells were gently washed away with 5 ml DI water using a pipette. After adding a drop of DI water containing the live/dead cell distinguishing stain, the chip was flipped, secured on a coverslip and loaded onto an inverted microscope for observation.

#### Electrical pulses and the antimicrobial efficiency

The electrical pulses were applied to the chip using a pulse generator (Avtech Electrosystems, AV-1010-B), which was triggered by a waveform generator (Keysight, 33509B). The pulse waveform was measured using an oscilloscope (Tektronix, DPO 5104) (Supplementary Fig. 12).

The applied electric field used in the figures and discussions is the background electric field, which is simply calculated by the equation EF = V/d, where V is the applied voltage and d is the distance separating the positive/negative electrodes. As the distance between the electrodes is subject to change in other studies and in practical applications, using the background electric field to represent the applied treatment strength makes it more convenient to compare with other studies (Supplementary Section 1.2). Pulses were delivered at a duty cycle of 0.1% (pulse width/period = 0.1%) to allow the membrane to fully discharge between pulses and avoid electrochemical reactions. In the experiments shown in Fig. 3b, both 1% and 0.1% duty cycles were tested, which corresponded to 500 kHz frequency (2  $\mu$ s period) and 50 kHz frequency (20  $\mu$ s period) for 20 ns pulses, and 5 kHz frequency (200  $\mu$ s period) and 0.5 kHz frequency (2 ms period) for 2  $\mu$ s pulses, respectively.

The antimicrobial efficiency of CEFT is the percentage of cells inactivated or damaged between the two electrodes. As CEFT is a homogeneous treatment process, the area of interest is the bulk space between the two electrodes (Supplementary Fig. 5a). The antimicrobial efficiency is calculated as the number of inactivated or damaged bacteria divided by the total number of bacteria between the two electrodes. The antimicrobial efficiency of LEEFT is represented by the percentage of nanowedges inducing bacteria damage or inactivation. Different from CEFT, LEEFT is a heterogeneous process. The area of interest (effective zone) is the nanowedge tips, not the whole bulk space between the two electrodes. Therefore, the percentage of the nanowedges that can induce bacteria inactivation is the best characterization of the antimicrobial efficiency of LEEFT (Supplementary Fig. 5b). There are 330 nanowedges on one chip. For both CEFT and LEEFT, each treatment condition was repeated three times with three chips. The error bars represent the standard deviation (s.d.) from the three replicates.

## Double staining method, oxidative stress detection, membrane lipid peroxidation detection and microscopy

Before treatment, the bacteria immobilized on chip were immersed in a drop of DI water containing 5  $\mu$ M live/dead cell viability stain SYTOX Green (Invitrogen). The cells damaged during the treatment would show green fluorescence. Twenty minutes after the treatment, PI (Invitrogen) was added at 15  $\mu$ M to stain the inactivated cells, which would show a red, orange or yellow fluorescence in the microscopy images (Supplementary Fig. 2). Reversible pores should already close within the 20 min window, so the cells stained with PI are considered to have permanent membrane damage and be inactivated  $^{15}$ .

To measure the bacterial cell oxidative stress, the cells were stained using a fluorescence probe DCFH-DA (Sigma-Aldrich) at 0.2 mM during the bacteria immobilizing process for 50 min (ref. 18). When electrical pulses are applied, the cells having oxidative stress will show a green fluorescence. Strong oxidation will result in stronger fluorescence in more cells. Therefore, the overall cell oxidative stress (Fig. 3b, top) was calculated as the product of the area of cells showing fluorescence and the mean DCFH-DA fluorescence intensity of the cells.

To assess lipid peroxidation, *S. epidermidis* cells were stained with 20  $\mu$ M BODIPY 581/591 C11 reagent (Invitrogen) for 50 min and then treated with electrical pulses. In the presence of lipid peroxides, the stained cells will show a fluorescence shift from red at -590 nm to green at -510 nm (ref. 39). The green/red ratio was calculated by averaging the green/red fluorescence ratio of ten cells exactly located at the tip of ten nanowedges. Higher ratio indicates more severe lipid peroxidation.

The bacteria were observed using an inverted fluorescence microscope (Zeiss Axio Observer 7). The cell and nanowedge images were captured via the Differential Interference Contrast (DIC) channel. PI was excited at 555 nm. SYTOX Green and DCFH-DA were excited at 488 nm. BODIPY 581/591 C11 was excited at both 488 nm (for green fluorescence) and 555 nm (for red fluorescence). All emission light was filtered by a 90 HS filter.

#### **Bacterial cell SEM imaging**

The bacteria immobilized on the chip surface were first fixed overnight in phosphate buffer (pH7.4) containing 2% glutaraldehyde and 2% paraformaldehyde (Electron Microscopy Sciences) at 4 °C. Subsequently, the sample was dehydrated in ethanol solution with increasing concentrations (50%, 70%, 90% and 100%) for 30 min per step, followed by critical point drying (Electron Microscopy Sciences Ltd. EMS850) (ref. 42). The samples were then sputter-coated with a thin layer of gold and observed using an SEM (Hitachi SU8230).

#### Electric field and TMV simulation

The nano-enhanced electric field and TMV were simulated using a finite element method in COMSOL Multiphysics 5.6. The electric current module was used for the simulation. Two concentric spheres were built to represent a bacterial cell with 1  $\mu m$  diameter and 50-nm-thick cell wall<sup>43</sup>. For the extracellular water, intracellular medium and cell membrane, the conductivity values were set at  $5\times10^{-4}$ , 0.2 and  $5\times10^{-7}$  S m $^{-1}$  (ref. 44), and the relative permittivity values were 78.5, 60 and 70, respectively $^{45}$ . Although most bacteria are negatively charged at a neutral pH, the resting TMV caused by this initial surface charge was ignored in the simulation. This is because the resting TMV ranges between approximately -0.14 and -0.075 V (ref. 46), which is much lower than the reported electroporation threshold (1 V) (ref. 47) and the TMV achieved in this simulation (for example, ~4 V at 12 kV cm $^{-1}$  applied electric field as shown in Fig. 4c).

#### **Data analysis**

All microscopy images were processed using scripts developed in MATLAB (version 2021b, MathWorks). The error bars on the data represent the s.d. derived from three independent tests with three chips.

### Data availability

The data supporting the findings of this study are available within the paper and Supplementary Information. Source data are provided with this paper. All other data are available from the authors on reasonable request.

#### Code availability

The scripts for data analysis were developed in MATLAB (version 2021b, MathWorks) and are available from the authors on reasonable request.

#### References

- Supply, W. U. J. W. & Programme, S. M. Progress on Sanitation and Drinking Water: 2015 Update and MDG Assessment (World Health Organization, 2015).
- Silvestry-Rodriguez, N., Sicairos-Ruelas, E. E., Gerba, C. P. & Bright, K. R. in Reviews of Environmental Contamination and Toxicology, Vol. 191 (ed. Ware, G.) 23–45 (Springer, 2007).
- Chen, W. et al. Silver nanowire-modified filter with controllable silver ion release for point-of-use disinfection. *Environ. Sci.* Technol. 53, 7504–7512 (2019).
- Lemire, J. A., Harrison, J. J. & Turner, R. J. Antimicrobial activity of metals: mechanisms, molecular targets and applications. *Nat. Rev. Microbiol.* 11, 371–384 (2013).
- Li, Q. et al. Antimicrobial nanomaterials for water disinfection and microbial control: potential applications and implications. Water Res. 42, 4591–4602 (2008).
- Zheng, K., Setyawati, M. I., Lim, T.-P., Leong, D. T. & Xie, J. Antimicrobial cluster bombs: silver nanoclusters packed with daptomycin. ACS Nano 10, 7934–7942 (2016).
- Howe, K. J., Crittenden, J. C., Hand, D. W., Trussell, R. R. & Tchobanoglous, G. Principles of Water Treatment (Wiley, 2012).
- Sedlak, D. L. & von Gunten, U. The chlorine dilemma. Science 331, 42–43 (2011).

- Zhang, Y., Gu, A. Z., He, M., Li, D. & Chen, J. Subinhibitory concentrations of disinfectants promote the horizontal transfer of multidrug resistance genes within and across genera. *Environ. Sci. Technol.* 51, 570–580 (2017).
- Lu, J. et al. Both silver ions and silver nanoparticles facilitate the horizontal transfer of plasmid-mediated antibiotic resistance genes. Water Res. 169, 115229 (2020).
- Operations, U. S. E. P. A. O. O. W. P. Alternative Disinfectants and Oxidants Guidance Manual. Vol. 99 (US Environmental Protection Agency, Office of Water, 1999).
- 12. You, J., Guo, Y., Guo, R. & Liu, X. A review of visible light-active photocatalysts for water disinfection: features and prospects. *Chem. Eng. J.* **373**, 624–641 (2019).
- 13. Pepper, I. L., Gerba, C. P., Gentry, T. J. & Maier, R. M. *Environmental Microbiology* (Academic Press, 2011).
- Zhou, J., Hung, Y.-C. & Xie, X. Making waves: pathogen inactivation by electric field treatment: from liquid food to drinking water. Water Res. 207, 117817 (2021).
- Kotnik, T., Rems, L., Tarek, M. & Miklavčič, D. Membrane electroporation and electropermeabilization: mechanisms and models. *Annu. Rev. Biophys.* 48, 63–91 (2019).
- Tieleman, D. P., Leontiadou, H., Mark, A. E. & Marrink, S.-J.
  Simulation of pore formation in lipid bilayers by mechanical stress and electric fields. J. Am. Chem. Soc 125, 6382–6383 (2003).
- Huang, K. & Wang, J. Designs of pulsed electric fields treatment chambers for liquid foods pasteurization process: a review. *J. Food Eng.* 95, 227–239 (2009).
- Wang, T., Brown, D. K. & Xie, X. Operando investigation of locally enhanced electric field treatment (LEEFT) harnessing lightning-rod effect for rapid bacteria inactivation. *Nano Lett.* 22, 860–867 (2021).
- 19. Liu, C. et al. Conducting nanosponge electroporation for affordable and high-efficiency disinfection of bacteria and viruses in water. *Nano Lett.* **13**, 4288–4293 (2013).
- 20. Zhou, J., Wang, T., Chen, W., Lin, B. & Xie, X. Emerging investigator series: locally enhanced electric field treatment (LEEFT) with nanowire-modified electrodes for water disinfection in pipes. *Environ. Sci. Nano* **7**, 397–403 (2020).
- Zhou, J., Wang, T. & Xie, X. Locally enhanced electric field treatment (LEEFT) promotes the performance of ozonation for bacteria inactivation by disrupting the cell membrane. *Environ*. Sci. Technol. 54, 14017–14025 (2020).
- 22. Huo, Z.-Y. et al. A  $Cu_3P$  nanowire enabling high-efficiency, reliable, and energy-efficient low-voltage electroporation-inactivation of pathogens in water. *J. Mater. Chem. A* **6**, 18813–18820 (2018).
- 23. Zhou, J., Wang, T., Yu, C. & Xie, X. Locally enhanced electric field treatment (LEEFT) for water disinfection. *Front. Environ. Sci. Eng* **14**, 78 (2020).
- Huo, Z.-Y. et al. Nanowire-modified three-dimensional electrode enabling low-voltage electroporation for water disinfection. *Environ. Sci. Technol.* 50, 7641–7649 (2016).
- 25. Cui, S., Chen, S., Wang, H., Dong, L. & Wang, S. N-doped carbon-coated  $\text{Cu}_7\text{S}_4$  nanowires on Cu foam supports for water disinfection. ACS Appl. Nano Mater. **4**, 6124–6134 (2021).
- 26. Wang, S. et al. Hierarchical  $\mathrm{Cu_2O}$  nanowires covered by silver nanoparticles-doped carbon layer supported on  $\mathrm{Cu}$  foam for rapid and efficient water disinfection with lower voltage. *Chem. Eng. J.* **382**, 122855 (2020).
- 27. Pi, S.-Y. et al. Fabrication of polypyrrole nanowire arrays-modified electrode for point-of-use water disinfection via low-voltage electroporation. *Water Res.* **207**, 117825 (2021).
- Huo, Z.-Y. et al. Triboelectrification induced self-powered microbial disinfection using nanowire-enhanced localized electric field. Nat. Commun. 12, 3693 (2021).

- Xie, X. et al. Nanostraw-electroporation system for highly efficient intracellular delivery and transfection. ACS Nano 7, 4351–4358 (2013).
- Vecitis, C. D., Zodrow, K. R., Kang, S. & Elimelech, M. Electronicstructure-dependent bacterial cytotoxicity of single-walled carbon nanotubes. ACS Nano 4, 5471–5479 (2010).
- 31. Wang, T., Chen, H., Yu, C. & Xie, X. Rapid determination of the electroporation threshold for bacteria inactivation using a lab-on-a-chip platform. *Environ. Int.* **132**, 105040 (2019).
- 32. Elbourne, A. et al. Antibacterial liquid metals: biofilm treatment via magnetic activation. ACS Nano 14, 802–817 (2020).
- Gao, F., Shao, T., Yu, Y., Xiong, Y. & Yang, L. Surface-bound reactive oxygen species generating nanozymes for selective antibacterial action. Nat. Commun. 12, 745 (2021).
- Loraine, G., Chahine, G., Hsiao, C.-T., Choi, J.-K. & Aley, P. Disinfection of Gram-negative and Gram-positive bacteria using DynaJets® hydrodynamic cavitating jets. *Ultrason*. Sonochem. 19, 710–717 (2012).
- 35. Virto, R., Manas, P., Alvarez, I., Condon, S. & Raso, J. Membrane damage and microbial inactivation by chlorine in the absence and presence of a chlorine-demanding substrate. *Appl. Environ. Microbiol.* **71**, 5022–5028 (2005).
- Slavin, Y. N., Asnis, J., Häfeli, U. O. & Bach, H. Metal nanoparticles: understanding the mechanisms behind antibacterial activity. *J. Nanobiotechnol.* 15, 65 (2017).
- Zhang, T. et al. Inactivation of bacteria by peracetic acid combined with ultraviolet irradiation: mechanism and optimization. Environ. Sci. Technol. 54, 9652–9661 (2020).
- Huang, X. et al. Investigation of functional selenium nanoparticles as potent antimicrobial agents against superbugs. *Acta Biomater*. 30, 397–407 (2016).
- Li, R. et al. Surface oxidation of graphene oxide determines membrane damage, lipid peroxidation, and cytotoxicity in macrophages in a pulmonary toxicity model. ACS Nano 12, 1390–1402 (2018).
- Kotnik, T., Bobanović, F. & Miklavčič, D. Sensitivity of transmembrane voltage induced by applied electric fields—a theoretical analysis. *Bioelectrochem. Bioenerg.* 43, 285–291 (1997).
- Zhou, J., Yu, C., Wang, T. & Xie, X. Development of nanowire-modified electrodes applied in the locally enhanced electric field treatment (LEEFT) for water disinfection. *J. Mater. Chem. A* 8, 12262–12277 (2020).
- 42. Xie, X. et al. Three-dimensional carbon nanotube-textile anode for high-performance microbial fuel cells. *Nano Lett.* **11**, 291–296 (2011).
- 43. Mai-Prochnow, A., Clauson, M., Hong, J. & Murphy, A. B. Gram positive and Gram negative bacteria differ in their sensitivity to cold plasma. Sci. Rep **6**, 38610 (2016).
- 44. Boukany, P. E. et al. Nanochannel electroporation delivers precise amounts of biomolecules into living cells. *Nat. Nanotechnol.* **6**, 747–754 (2011).

- 45. Sanchis, A. et al. Dielectric characterization of bacterial cells using dielectrophoresis. *Bioelectromagnetics* **28**, 393–401 (2007).
- Stratford, J. P. et al. Electrically induced bacterial membranepotential dynamics correspond to cellular proliferation capacity. *Proc. Natl Acad. Sci. USA* 116, 9552–9557 (2019).
- 47. Shahini, M. & Yeow, J. T. Cell electroporation by CNT-featured microfluidic chip. *Lab Chip* **13**, 2585–2590 (2013).

### Acknowledgements

The authors acknowledge the financial support from the National Science Foundation (grant number CBET 1845354). This work was performed in part at the Georgia Tech Institute for Electronics and Nanotechnology, a member of the National Nanotechnology Coordinated Infrastructure (NNCI), which is supported by the National Science Foundation (grant ECCS-2025462). T.W. is grateful for the financial support provided by the China Scholarship Council. T.W. also thanks X. Li for her assistance on the drawing included in Fig. 4.

#### **Author contributions**

X.X. and T.W. designed the research. T.W. performed the research. T.W. and X.X. analysed the data and wrote the paper.

#### **Competing interests**

The authors declare no competing interests.

#### **Additional information**

**Supplementary information** The online version contains supplementary material available at https://doi.org/10.1038/s44221-022-00003-2.

**Correspondence and requests for materials** should be addressed to Xing Xie.

**Peer review information** *Nature Water* thanks the anonymous reviewers for their contribution to the peer review of this work.

**Reprints and permissions information** is available at www.nature.com/reprints.

**Publisher's note** Springer Nature remains neutral with regard to jurisdictional claims in published maps and institutional affiliations.

Springer Nature or its licensor (e.g. a society or other partner) holds exclusive rights to this article under a publishing agreement with the author(s) or other rightsholder(s); author self-archiving of the accepted manuscript version of this article is solely governed by the terms of such publishing agreement and applicable law.

@ The Author(s), under exclusive licence to Springer Nature Limited 2023

#### **Table of Contents**

#### 1. Additional methods

- 1.1. Chip fabrication and pretreatment
- 1.2. Calculation of the applied electric field

## 2. Additional discussion

- 2.1. Energy consumption in nanosecond LEEFT
- 2.2. Water ionization and bubble formation in LEEFT
- 2.3. Electrochemical oxidation in nanosecond LEEFT
- 2.4. Membrane charging and electroporation process
- 2.5. Membrane charging process when not contacting the nanowedge

### 3. Supplementary figures

- Figure S1. Photos of the chip and the experimental setup.
- Figure S2. A schematic of the double staining method with SYTOX Green and PI stain.
- Figure S3. Side-by-side comparison of the optical microscopy images and SEM images for bacteria inactivation by LEEFT using different treatment conditions.
- Figure S4. Simulation of the enhanced electric field of nanotip structures on chip.
- Figure S5. The area of interest for CEFT and LEEFT.
- Figure S6. Relative energy consumption of 20 ns pulses at different applied electric field.
- Figure S7. PI fluorescence intensity indicating quick pore closure in the cells located at the tips of the non-connected nanowedges.
- Figure S8. The stack fluorescence microscopy image of DCFH-DA and PI stained bacteria.
- Figure S9. Analysis and microscopy imaging of cell membrane peroxidation.

Figure S10. Electroporation process and membrane charging speed analysis.

Figure S11. The normalized TMV changed with charging time.

Figure S12. Waveform of a single electrical pulse.

#### 1. Additional methods

## 1.1. Chip fabrication and pretreatment

To fabricate the gold nanowedges, a layer of electron beam resist PMMA A6 was spin-coated on the surface of a glass wafer substrate. Then, the substrate was exposed using an electron beam lithography system (Elionix ELS-G100). After development, a thin layer of gold (200 nm) was deposited using an e-beam evaporator (Denton Explorer). The unwanted gold was removed by a lift-off method using acetone, leaving the gold nanowedges on the substrate. After the nanowedges were fabricated, the 300 nm thick bulk gold electrodes with 25 or 50 µm electrode separation gap were fabricated using a similar procedure except that photolithography was used rather than e-beam lithography. A layer of photoresist (NR9-1500py) was first spin coated on the substrate, then exposed by photolithography (Heidelberg MLA150), and the gold was deposited by e-beam evaporator and lift-off method.

To achieve bacteria immobilization on the chip, the fabricated chips were first washed with 5% bleach for 30 min, rinse with DI water, washed with 30% H<sub>2</sub>O<sub>2</sub> for 1 hour, stored in DI water overnight, and then dried in oven before treatment. The dried chips were then coated with positively charged poly-L-lysine (0.01%, mw 150,000-300,000; Sigma-Aldrich) for bacteria immobilization. Specifically, poly-L-lysine and 2 M borate buffer was first mixed at 1:1, then about 50 μL of the mixture was added onto the center of a dried chip, covering the gap between the two electrodes. After 3 hours of coating at room temperature, the chips were rinsed with DI water and dried in 60 °C for 20 min. The coated chips were stored in 4 °C to avoid coating layer degradation. Poly-L-lysine is a positively charged polymer, which can immobilize the negatively charged bacteria on the chip surface. To reuse the chips after experiments, repeat the wash and coating steps.

## 1.2. Calculation of the applied electric field

The applied electric field used in the figures and discussion is the background electric field, which is calculated by the equation, EF = V/d, where V is the applied voltage and d is the distance separating the positive/negative electrodes. Since the electrode separation distance is subject to change in other studies and in real applications, same applied voltage may yield very different electric field. Therefore, the background electric field is widely used in electric field treatment to represent the applied treatment strength. For LEEFT, the electric filed at the tip ( $E_{tip}$ ) is enhanced roughly estimated by **Equation S1**:

$$E_{\rm tip} = a \cdot \frac{L_{\rm nanowedge}}{D_{\rm nanowedge}} \cdot E_{\rm background}$$
 (S1)

where  $E_{\rm background}$  is the background electric field,  $L_{\rm nanowedge}$  and  $D_{\rm nanowedge}$  is the length and width of the nanowedge, and a is a constant.<sup>2</sup> The exact electric field at the nanowedge tip is affected by some factors, such as the exact shape and material of the nanowedge. Therefore, using the background electric field to represent the applied treatment strength is more general, and makes it more convenient to compare with other studies.

#### 2. Additional discussion

## 2.1. Energy consumption in nanosecond LEEFT

For nanosecond LEEFT, applying a stronger electric field can greatly reduce energy consumption (**Figure S6**). It is because by slightly increasing the applied electric field, the effective treatment time can be shortened by several orders of magnitude (**Figure 2d**). This property is different from the chemical-based antimicrobial methods relying on oxidation, where increasing the chemical dosage only allows a similar scale of treatment time decrease, so that the product of dosage and time (*i.e.*, the CT value) remains similar for a certain disinfection efficiency.<sup>3</sup> It can be explained by the inherent mechanism difference between electroporation and oxidation. For electroporation, the cells cannot be perforated if the electric field does not reach a threshold, no matter how long the electrical pulse is and how many pulses are applied. However, once pores are induced by a strong electric field, a short effective treatment time is sufficient to inactive the bacteria, which can reduce the energy consumption by several orders of magnitude.

### 2.2. Water ionization and bubble formation in LEEFT

There should be no water ionization events causing cell inactivation, since the breakdown strength of water is higher than 2 MV/cm with the pulse width <50 ns,<sup>4, 5</sup> which is much higher than the highest applied electric field in this work (55 kV/cm) and the nano-enhanced electric field at the nanowedge tips (<1000 kV/cm). Bubbles were only formed under very strong treatment conditions where severe oxidative stress has already been detected (denoted by \* in **Figure 3b**). In this study, there was no bubble formation under 20 ns pulses even at 55 kV/cm.

#### 2.3. Electrochemical oxidation in nanosecond LEEFT

Nanosecond pulses induce less oxidative stress than longer pulses (**Figure 3b**), meaning that the ultrashort pulses are less likely to induce electrochemical reactions under the same voltage and

duty cycle. Although electrochemical reactions may cause more bacteria inactivation, they raise problems including water splitting and generating disinfection by-products (DBPs), thus deteriorating the water quality. With nanosecond pulses, a stronger electric field and higher frequencies could be applied to achieve more efficient bacteria inactivation, while maintaining pristine electroporation, eliminating unwanted side reactions, and minimizing DBP generation. Ultrafast nanosecond pulses are also safer to operate, which makes the approach more applicable for real-world water disinfection applications.

## 2.4. Membrane charging and electroporation process

The electroporation processes are shown in **Figure S10a**. When the cell is exposed to an external electric field E, the charged ions in the cytoplasm and extracellular medium will migrate and accumulate at the two sides of the membrane, generating an induced TMV ( $\Delta V$ ). When the TMV reaches a certain threshold, water molecules penetrate the membrane, generating a water column and the hydrophobic pore. Then, the lipids rearrange their head group toward the water column, generating the hydrophilic pore. Charging the cell membrane by ions is like charging a capacitor in a circuit, where C is the membrane capacitance, and  $R_i$ ,  $R_e$ ,  $R_m$  are the resistance of the cytoplasm, extracellular medium, and the membrane (**Figure S10b**).

The TMV induced by the external electric field ( $\Delta V$ ) is given in **Equation S2**:<sup>6</sup>

$$\Delta V = f_{\rm s} r E cos\theta \left[ 1 - exp \left( -\frac{t}{\tau} \right) \right] \tag{S2}$$

where  $f_s$  is a factor related to the electric field and properties of the cell and medium, r is the cell radius, E is the external electric field strength,  $\theta$  is the angle between the direction of electric field and the point of interest, t is the pulse width, and  $\tau$  is the RC time constant of the membrane, which is the time required to charge the membrane to 63.2% of the maximum possible TMV. The membrane charging constant  $\tau$  is further determined by **Equation S3**:6

$$\tau = \frac{rC_{\rm m}}{\left(\frac{2\sigma_{\rm e}\sigma_{\rm i}}{2\sigma_{\rm e} + \sigma_{\rm i}}\right) + \frac{r}{d}\sigma_{\rm m}}$$
 (S3)

where r is the cell radius,  $C_{\rm m}$  is the surface capacitance of the membrane,  $\sigma_{\rm i}$ ,  $\sigma_{\rm e}$ , and  $\sigma_{\rm m}$  are the conductivities of the cytoplasm, the extracellular medium, and the membrane, respectively, and d is the thickness of membrane. According to the values reported in literature, the  $f_{\rm s}$ ,  $\sigma_{\rm i}$ ,  $\sigma_{\rm m}$ ,  $C_{\rm m}$ , d, and r are 1.5, 0.2 S/m,  $5\times10^{-6}$  S/m, 0.01 F/m<sup>2</sup>, 50 nm, and 0.5  $\mu$ m, respectively.<sup>6</sup> The relationship between the membrane charging constant  $\tau$  and the extracellular medium conductivity  $\sigma_{\rm e}$  is shown in **Figure S10c**. The charging constant increases with the decrease of conductivity, meaning that longer time is needed to charge the membrane when the extracellular medium conductivity is low. The dependence of the membrane charging percentage on the pulse width under different medium conductivities is shown in **Figure S10d**. Tens of nanoseconds can only charge the membrane to <50%, especially under low conductivities. The conductivities of DI water, tap water, and juice are around  $5\times10^{-5}$ ,  $1\times10^{-2}$ , and  $3\times10^{-1}$  S/m, respectively.<sup>7</sup>

## 2.5. Membrane charging process when not contacting the nanowedge

For the cells not directly contacting the nanowedge tip, the membrane still needs to be charged by the ions in the medium between the cell and the tip. In this case, the charging speed will be affected by both the strength of the locally enhanced electric field, which is determined by the distance of the cells away from the nanowedge tips, and the conductivity of the medium. When the cells are very close to the nanowedge tips (*e.g.*, less than a few hundred nanometers) and the medium conductivity is not very low, inactivation in nanoseconds may still be possible. Nevertheless, the direct cell-nanowedge contact guarantees the fastest membrane charging, which is critical for the nanosecond cell electroporation and inactivation in LEEFT.

## 3. Supplementary figures

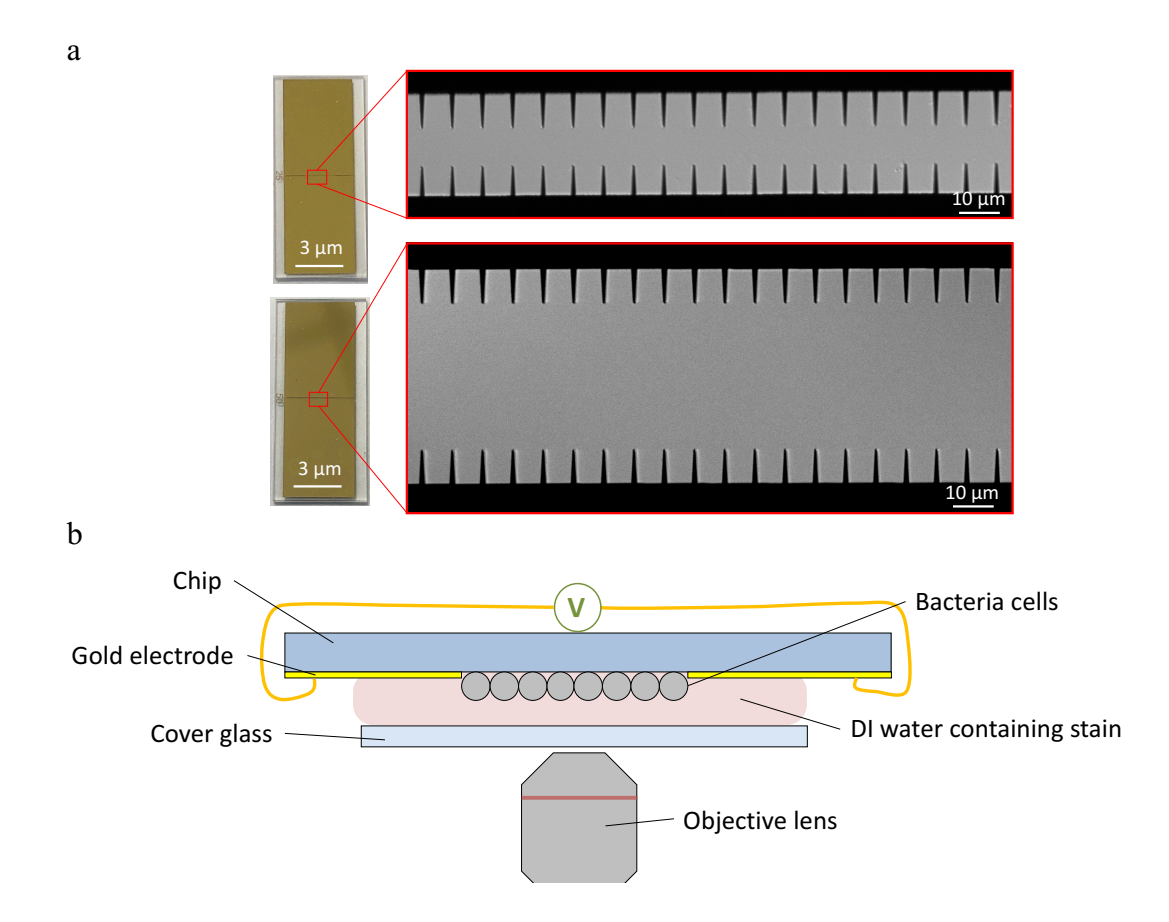


**Figure S1.** Photos of the chip and the experimental setup. (a) Digital photos and optical microscopy images of the lab-on-a-chip with 20  $\mu$ m or 50  $\mu$ m gap between the two electrodes. (b) The experimental setup. The cells are immobilized on the chip surface. The medium is DI water containing SYTOX Green or PI stain.

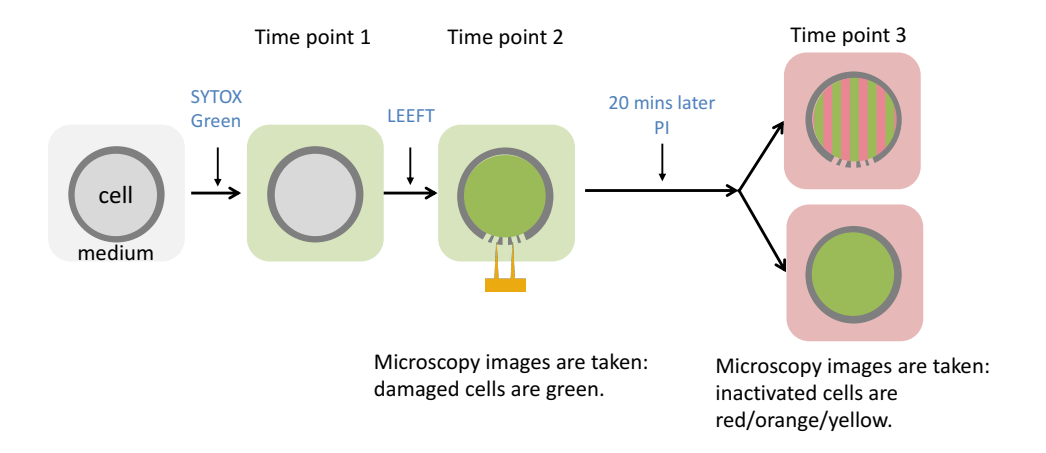
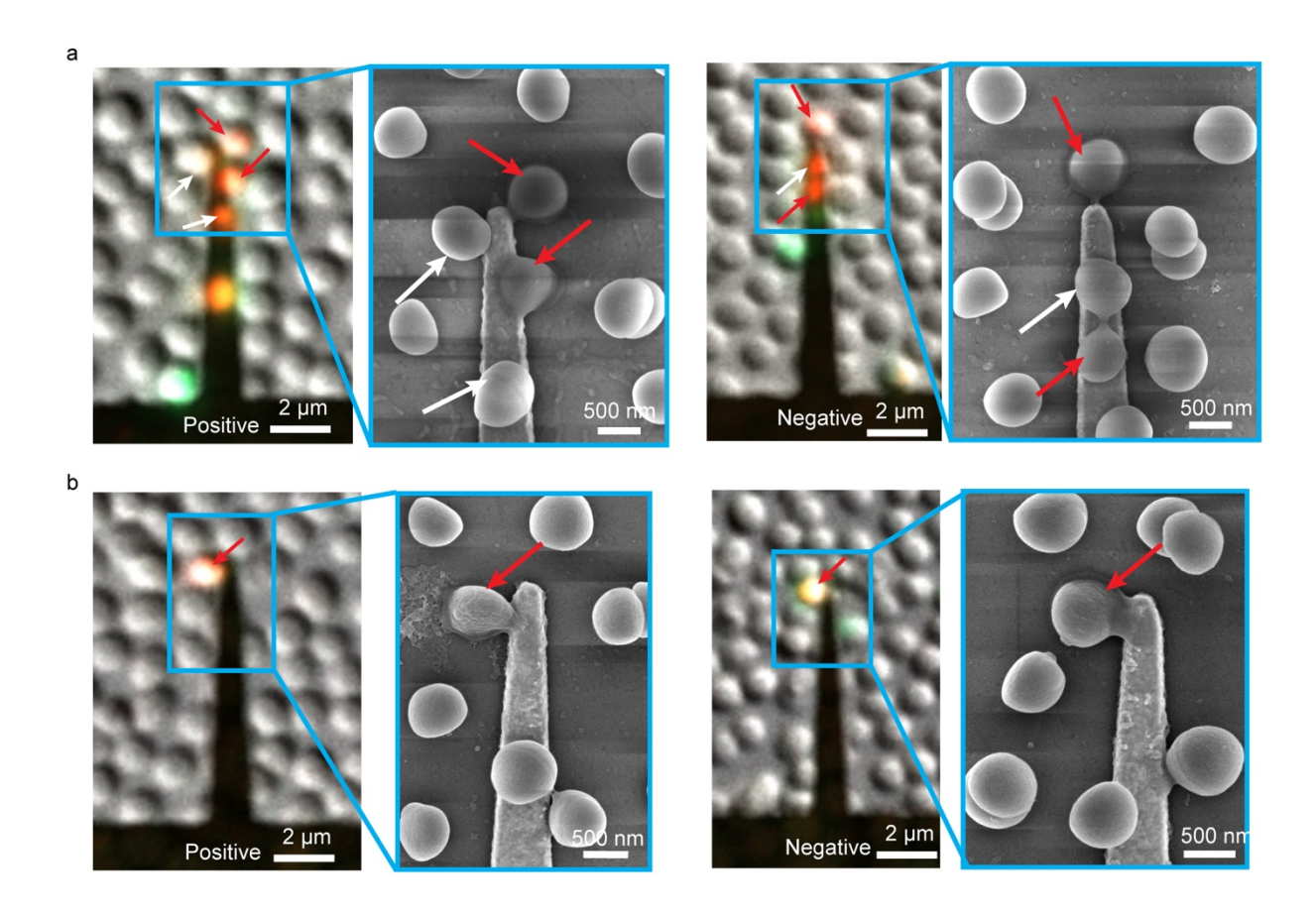
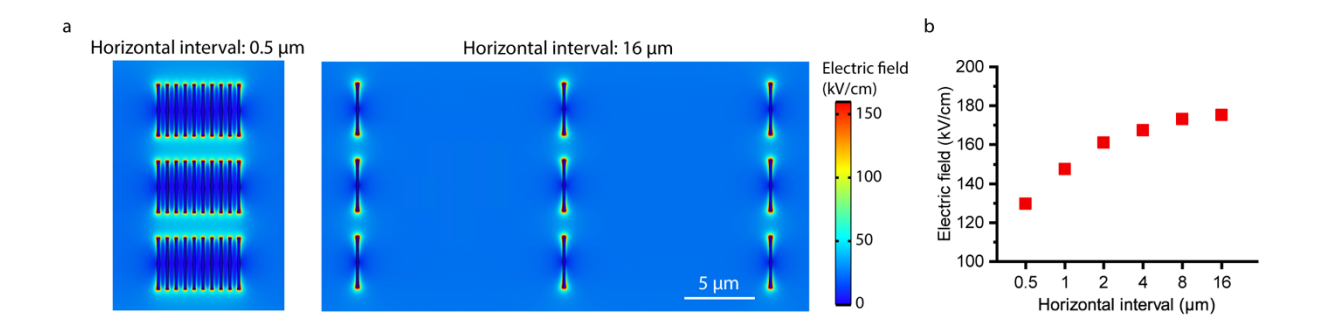


Figure S2. A schematic of the double staining method with SYTOX Green and PI stain.



**Figure S3.** Side-by-side comparison of the optical microscopy images and SEM images for bacteria inactivation by LEEFT using (a) 20 ns pulses at 22 kV/cm with 20  $\mu$ s effective treatment time and (b) 20 ns pulses at 12 kV/cm with 20 ms effective treatment time.



**Figure S4.** Simulation of the enhanced electric field of nanotip structures on chip. (a) Simulation images of the nanotip structures on chip with different horizontal interval. (b) The nano-enhanced electric field over the horizontal interval between nanotip structures.

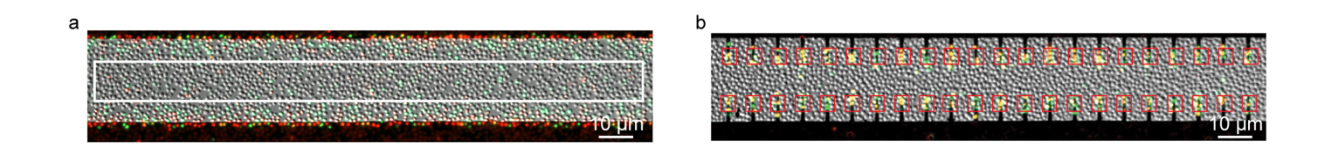


**Figure S5.** The area of interest for CEFT and LEEFT. (a) The white rectangle is the area of interest for CEFT, which is to investigate the antimicrobial efficiency in the bulk space between the two electrodes. The antimicrobial efficiency of CEFT is calculated as the percentage of cells inactivated or damaged between the two electrodes in the white rectangle. The image was taken after 20 ns pulses at 55 kV/cm for 200 ms effective treatment time. More bacteria are damaged or inactivated at the electrode edge, which is induced by the electric field enhancement due to the thin electrode edge (300 nm thick). However, in practical applications, the electrodes are two parallel plates, where there is no sharp edge and significant electric field enhancement. So, the area of interest (white rectangle) is defined to consider the bulk space and avoid the area affected by the edge. (b) The nanowedge tips are the effective zones of LEEFT, so that the red squares are the area of interest for LEEFT. The antimicrobial efficiency of LEEFT is represented by the percentage of nanowedges inducing bacteria damage or inactivation, which is calculated by the number of nanowedges have damaged/dead bacteria at the tip after treatment divided by the total number of nanowedges. The image was taken after 20 ns pulses at 40 kV/cm for 200 ns effective treatment time.

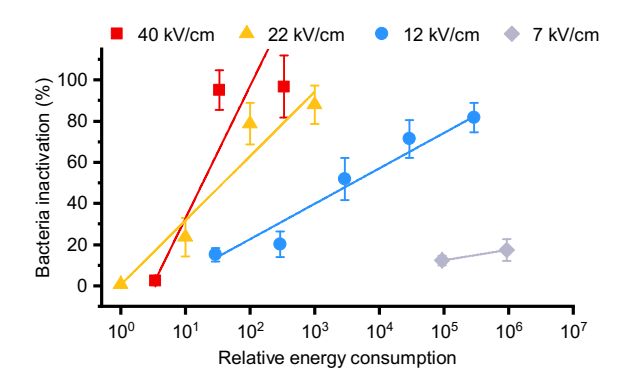


**Figure S6.** Relative energy consumption of 20 ns pulses at different applied electric field. The energy consumption J is calculated by  $J = n \int_{t_1}^{t_2} VI(t)dt$ , where V is the applied voltage, I is the current,  $t_1$ ,  $t_2$  is the starting and ending time of one pulse, t is time, and t is the pulse number. The relative energy consumption is calculated by normalizing all data to the smallest t value. Data are presented as mean values. Error bars represent the s.d. from t = 3 replicates.

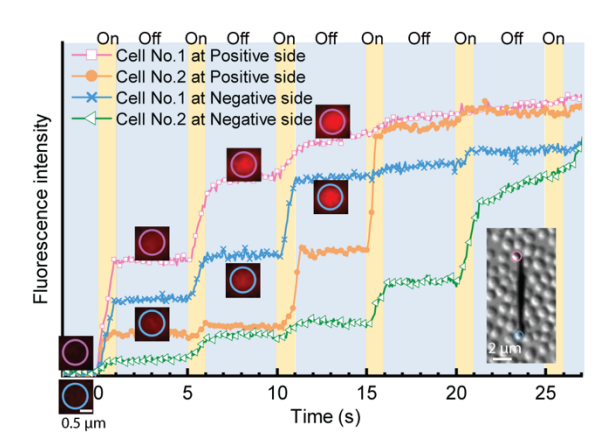


**Figure S7.** PI fluorescence intensity indicating quick pore closure in the cells located at the tips of non-connected nanowedges. The "on" (yellow area) indicates 20 ns pulses at 12 kV/cm for 1 s. The "off" (blue area) indicates 0 V for 4 s. The insets are optical microscopy images of the cell.

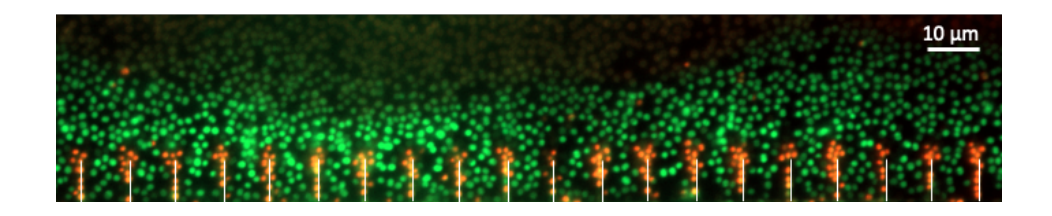
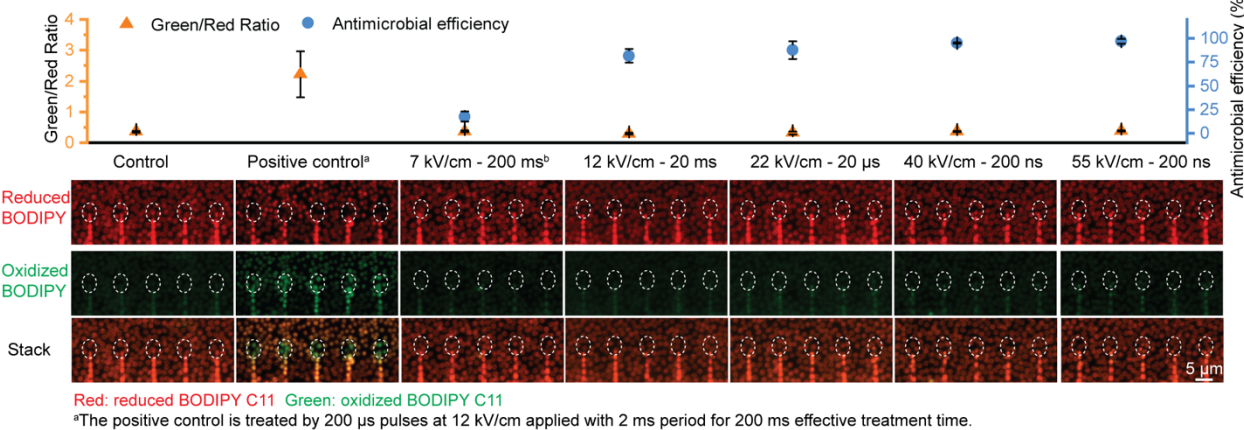


**Figure S8.** The stack fluorescence microscopy image of DCFH-DA stained cells (green, indicating oxidative stress) and PI stained cells (red, indicating cell inactivation) after LEEFT of 20 ns/500 kHz at 22 kV/cm for 20 ms effective treatment time. The green cells have oxidative stress, but not all of them are inactivated. This indicates that even significant oxidative stress is detected in some cells, it does not necessarily cause bacteria inactivation.



The positive control is treated by 200 μs pulses at 12 kV/cm applied with 2 ms period for 200 ms effective treatment time b7 kV/cm is the applied electric field, 20 ms is the effective treatment time.

**Figure S9.** Analysis and microscopy imaging of cell membrane peroxidation under 20 ns pulse treatment. To assess lipid peroxidation, S. staphylococcus were stained with 20 µM BODIPY 581/591 C11 reagent and then treated with 20 ns pulses at several different applied electric field and effective treatment times. In the presence of lipid peroxides, the stained cells will show a green shift in fluorescence activity from red at ~590 nm to green at ~510 nm. The Green/Red Ratio is calculated by averaging the green/red fluorescence of 10 cells located exactly at the tip of 10 nanowedge. Higher ratio indicates more sever lipid peroxidation. The results show that the cell Green/Red Ratio after treated with 20 ns pulses stays the same with the control group, which are significantly lower than the positive control group, indicating that no significant lipid peroxidation is detected under 20 ns pulses. The corresponding antimicrobial efficiencies are the same as the data shown in Figure 2d. No significant membrane peroxidation is detected even though around 90% bacteria inactivation is achieved, indicating that the bacteria inactivation is not due to extracellular ROS generation or membrane peroxidation. Data are presented as mean values. Error bars represent the s.d. from n = 3 replicates.

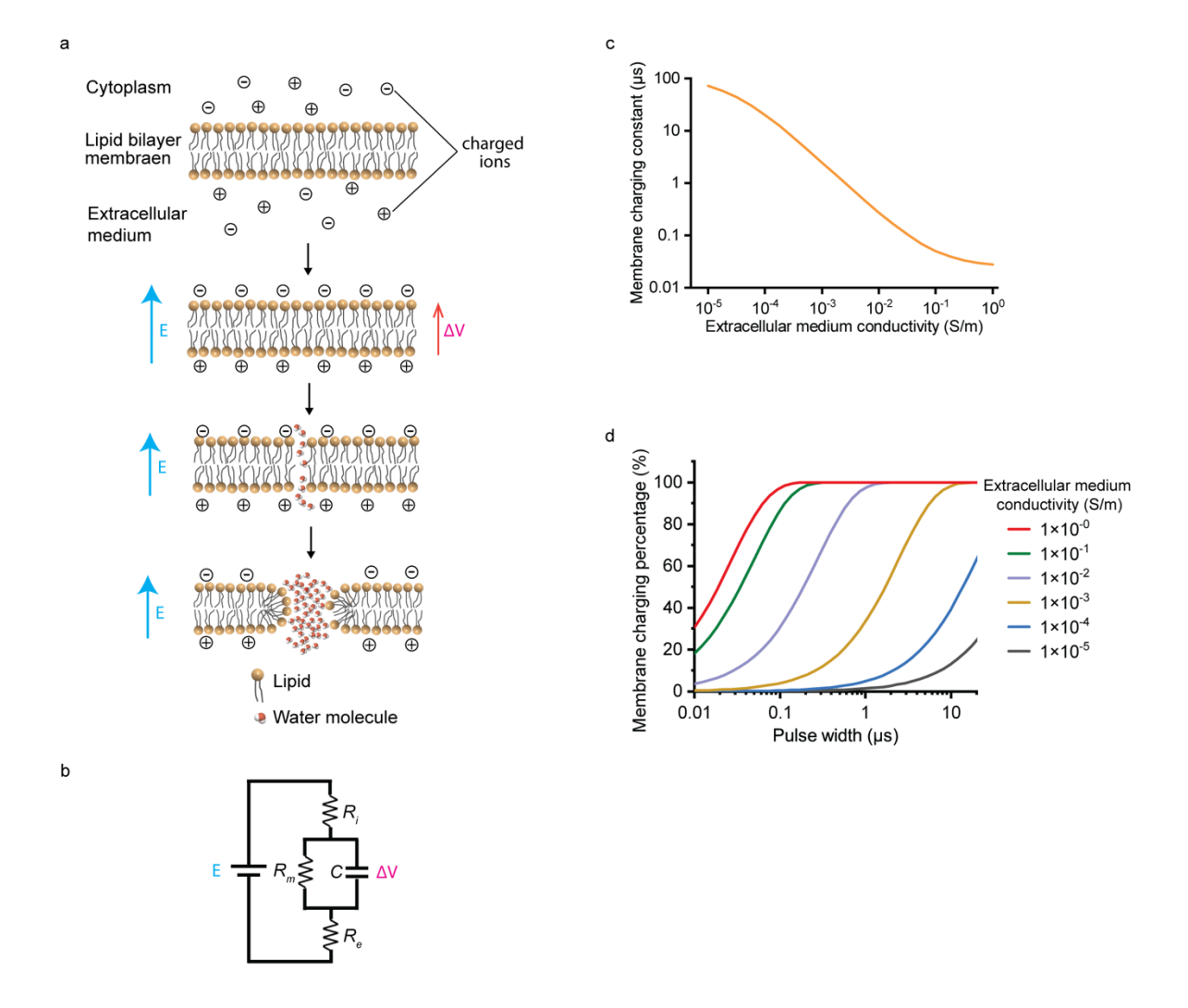


**Figure S10.** Electroporation process and membrane charging speed analysis. (a) A schematic of the electroporation process. When the lipid bilayer membrane is exposed to an external electric field E, charged ions accumulate on the two sides of the membrane, generating an induced TMV ( $\Delta V$ ). Then, water molecules orient their dipoles along the transmembrane voltage, forming a water column across the lipid bilayer. The lipids will rearrange their hydrophilic head group toward the water column, generating the hydrophilic pore. (b) The equivalent electrical circuit of the cell membrane charging.  $R_i$ ,  $R_e$ ,  $R_m$ , and C is the resistance of cytoplasm, extracellular medium, membrane, and the capacitance of the membrane. (c) The relationship between the membrane

charging constant  $\tau$  and the extracellular medium conductivity  $\sigma_e$ . (d) The dependence of the membrane charging percentage on the pulse width under different medium conductivities.

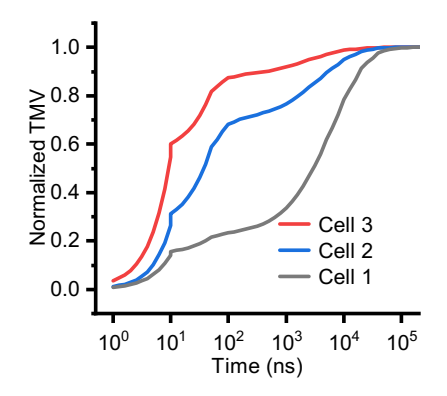


Figure S11. The normalized TMV representing the charging ratio changed with charging time.

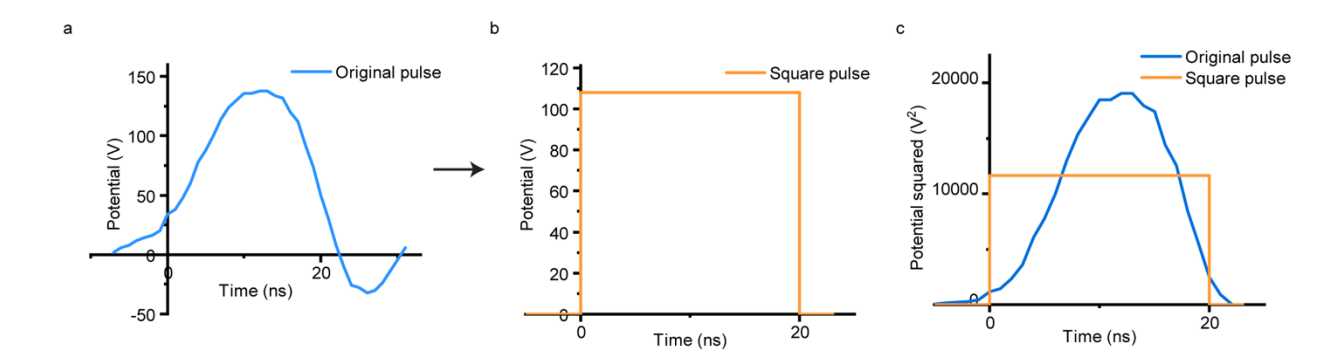


Figure S12. Waveform of a single electrical pulse. (a) The original pulse is a peak due to the short pulse width. (b) The peak is represented as a square pulse at the root mean square (RMS) voltage, which is 108.1 V (22 kV/cm when applied to 50  $\mu$ m). (c) The RMS voltage is calculated by the equation  $V_{\rm RMS} = \sqrt{\frac{1}{T} \int_{t_1}^{t_2} V^2(t) dt}$ , where T is 20 ns,  $t_1$ ,  $t_2$  are the starting and ending time of the peak, V is potential, and t is time. The area under the original pulse voltage square (blue line) equals to the area under square pulse voltage square (orange line).

#### REFERENCES

- 1. Maher, M.; Pine, J.; Wright, J.; Tai, Y.-C., The neurochip: a new multielectrode device for stimulating and recording from cultured neurons. *Journal of neuroscience methods* **1999**, *87*, (1), 45-56.
- 2. Rojas-Chapana, J. A.; Correa-Duarte, M. A.; Ren, Z.; Kempa, K.; Giersig, M., Enhanced introduction of gold nanoparticles into vital acidothiobacillus ferrooxidans by carbon nanotube-based microwave electroporation. *Nano Letters* **2004**, *4*, (5), 985-988.
- 3. Howe, K. J.; Crittenden, J. C.; Hand, D. W.; Trussell, R. R.; Tchobanoglous, G., *Principles of water treatment*. John Wiley & Sons: 2012.
- 4. Katsuki, S.; Xiao, S.; Joshi, R. P.; Laroussi, M.; Schoenbach, K. H. In *Electrical breakdown of sub-millimeter water gaps*, Conference Record of the Twenty-Fifth International Power Modulator Symposium, 2002 and 2002 High-Voltage Workshop., 2002; IEEE: 2002; pp 199-202.
- 5. Schoenbach, K.; Kolb, J.; Xiao, S.; Katsuki, S.; Minamitani, Y.; Joshi, R., Electrical breakdown of water in microgaps. *Plasma Sources Science and Technology* **2008**, *17*, (2), 024010.
- 6. Kotnik, T.; Bobanović, F.; Miklavc Ic, D., Sensitivity of transmembrane voltage induced by applied electric fields—A theoretical analysis. *Bioelectrochemistry* **1997**, *43*, (2), 285-291.
- 7. Icier, F.; Ilicali, C., The effects of concentration on electrical conductivity of orange juice concentrates during ohmic heating. *European Food Research and Technology* **2005**, *220*, (3), 406-414.